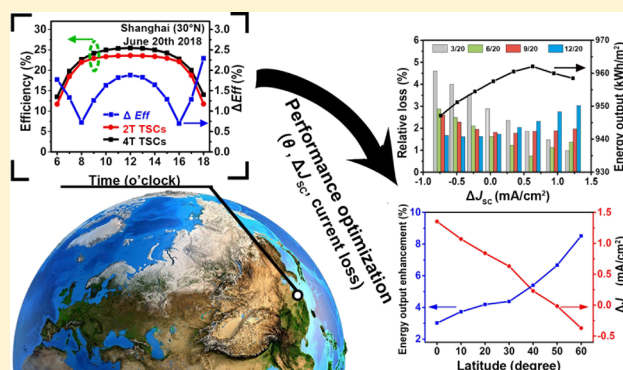


Perovskite/c-Si Monolithic Tandem Solar Cells under Real Solar Spectra: Improving Energy Yield by Oblique Incident Optimization

Lixiang Ba,[†] Tun Wang,[†] Jiayuan Wang,[†] and Wenzhong Shen^{*,†,‡}[†]Institute of Solar Energy, and Key Laboratory of Artificial Structures and Quantum Control (Ministry of Education), School of Physics and Astronomy, Shanghai Jiao Tong University, Shanghai 200240, People's Republic of China[‡]Collaborative Innovation Center of Advanced Microstructures, Nanjing 210093, Jiangsu, People's Republic of China

ABSTRACT: Many research groups have noticed the performance of rapidly developed perovskite/silicon monolithic tandem solar cells (TSCs) under a real situation, but they overlook the short current density mismatch of two subcells at different times in a day and the spectrum variation at different latitudes. Here, we have systematically analyzed the efficiency losses and proposed an optimization scheme by combination of the experiment and simulation relying on reliable experimental data in a year. We have verified the simulated absorptance spectra varying with incident angle θ to substitute the external quantum efficiency spectra, which makes the optimization at oblique incidence possible. More importantly, we have further calculated and expanded the optimized current losses and energy output enhancement in perovskite/silicon monolithic TSCs to all latitudes. This work can serve as a practical guidance for the design of perovskite/silicon monolithic TSCs with the best annual energy output at different latitudes in the world.



1. INTRODUCTION

In recent years, perovskite/silicon tandem solar cells (TSCs) have attracted tremendous concern in photovoltaics because of low-cost, high conversion efficiency potential, and high compatibility of preparation technologies.^{1–3} According to device architectures, perovskite/silicon TSCs can be classified to three types: monolithic integrated two-terminal (2T) TSCs, three-terminal (3T) TSCs, and mechanically stacked four-terminal (4T) TSCs. Because of less complexity and fewer transparent electrodes, 2T configuration has better feasibility in application fields than 3T and 4T architectures.^{1–6} The efficiencies of 2T TSCs^{7–14} have increased from 13.7%⁷ in 2015 to 23.6%¹⁰ in 2018 by employing better transport materials and a more suitable band gap. Soon Sahli et al. have reported a 25.2% efficiency perovskite/silicon monolithic TSC by using a new hybrid two-step perovskite deposition method to achieve conformal growth of multiple-compound perovskite on micrometer-sized pyramids.¹¹ Recently, Köhnen et al. have reported a high efficiency 2T TSC with an efficiency of 26% by seeking a balance between the current mismatch and the fill factor (FF).¹³ The efficiency losses caused by reflection, current mismatch, and parasitic absorption in transparent electrodes and transport materials of 2T TSCs can be further optimized in order to approach an efficiency limit of 43%.¹⁵ More conventional and feasible perovskite preparation methods on a textured silicon surface are absolutely necessary to be found, which will play an important role in the highly efficient perovskite/silicon monolithic TSCs.

Nowadays, the perovskite/silicon TSC technologies are becoming more and more mature for industrialization. On the one hand, the best efficiencies for both 2T and 4T configurations are over 27%, exceeding the present record efficiency of 26.7% in silicon solar cells,¹⁶ where some companies have contributed leading positions in the research and development of perovskite/silicon TSCs. Oxford PV has achieved certified 28% efficient perovskite/silicon 2T TSCs with 1 cm² cell area.¹⁷ IMEC has reported 27.1% efficient perovskite/silicon 4T TSCs with 0.13 cm² cell area.¹⁸ On the other hand, the efforts to amplify the cell area of perovskite/silicon monolithic TSCs are also on the way. Shali et al. have demonstrated a 12.96 cm² monolithic tandem cell with a steady-state efficiency of 18% by using nanocrystalline silicon recombination junction.¹⁹ Zheng et al. have employed a new front top metal grid design to increase the cell area to 16 cm² with an efficiency of 21.8%.²⁰ Kamino et al. have fabricated large area perovskite/c-Si TSCs with a steady-state efficiency of 22.6% over an aperture area of 57.4 cm² with a two-bus bar metallization pattern by a screen-printing process.²¹

The rapid progress in the industrialization of perovskite/silicon TSCs has already yielded the notice on the performance of perovskite/silicon TSCs under a real situation. Dupré et al. have evaluated annual losses because of differences by varying

Received: October 30, 2019

Revised: November 3, 2019

Published: November 5, 2019

light intensity, module temperature, and spectrum on Denver at vertical incidence.²² Jošt et al. have calculated the yearly energy yield for 2T TSCs with different textured foil at fixed solar cell orientation/inclination.²³ Schmager et al. have proposed a framework that enables detailed calculation of power output under realistic irradiation conditions by employing a simple cloud model.²⁴ Nevertheless, these considerations have not focused on how to balance the short-current density (J_{SC}) mismatch of two subcells at different times in a day and the spectrum variation at different latitudes. In this study, we have thoroughly analyzed the efficiency losses of perovskite/silicon monolithic TSCs at different times under clear-sky conditions in a year, and proposed an optimization scheme by the combination of experiment and simulation relying on reliable experimental data. Based on our previous theoretical work^{25–28} and experimental measurement for two individual subcells, we have verified the simulated absorptance spectra varying with incident angle θ to substitute the external quantum efficiency (EQE) spectra, which makes the optimization at oblique incidence possible. By combining oblique incidence with a quasi-omnidirectional pyramid textured front surface, we have proposed for the first time a method to make the output of perovskite/silicon monolithic TSCs during the mid-part of the days as large as possible and meanwhile minimize the losses during early and late day. Furthermore, we have also expanded the study to all latitudes and calculated the corresponding optimized current losses and energy output enhancement in perovskite/silicon 2T TSCs. This work will benefit for the design of perovskite/silicon monolithic TSCs with the best annual energy output at different latitudes in the world.

2. EFFICIENCY LOSSES AT VERTICAL INCIDENCE

For perovskite/silicon monolithic TSCs, many researchers have fabricated the best current match solar cell under the AM 1.5 G spectrum (standard test conditions).^{7–12,17} However in practical application, the spectrum changes all the time because the position of the sun and the atmospheric properties vary with time and geographic position such as the sun elevation angle, the sun zenith angle, temperature, pressure, precipitable water, ozone, and albedo.²⁹ Because there is still no unified, comprehensive radiative transfer model for clouds and diffuse light so far,²⁴ the real solar spectra that we chose is under clear-sky conditions, where direct light contributes a significant portion of the overall irradiation. To evaluate the influence of varying spectra, we have calculated J_{SC} and efficiency based on real perovskite/silicon monolithic TSCs under real solar spectra. First, we assumed that the module plane was always vertical to the sun light which can be easily achieved by tuning tilt and azimuth angles. The tilt angle was the angle between the plane of the module and horizontal, while the azimuth angle was the angle between the plane of the module and due north.³⁰ Then, we chose our university location Shanghai (latitude $\approx 30^\circ\text{N}$, longitude $\approx 120^\circ\text{E}$) as an example with the real simulated solar spectra under clear-sky conditions at different dates and sidereal time obtained from the website PVLighthouse.com. Other parameters had default values (including transmission model: SPCTRAL2 [Bir86]/atmospheric pressure: 1013.25 mb/turbidity at 500 nm: 0.084/precipitable water vapour: 1.4164 cm/ozone: 0.3438 atm cm/albedo: 0.1). As an example, Figure 1a shows the solar spectral irradiance with time ranging from 6 to 12 o'clock on June 20, 2018 in Shanghai 30°N . We took the maximum point at each

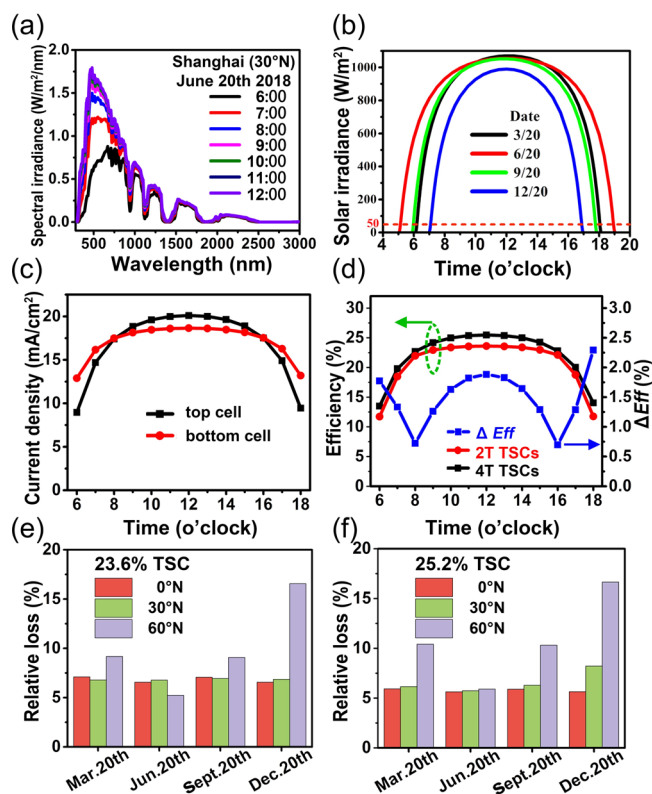


Figure 1. (a) Solar spectral irradiance varying with time on June 20, 2018 in Shanghai. (b) Solar irradiance on March 20, June 20, Sept 20, and Dec 20, 2018 in Shanghai. (c) Calculated current density of the top perovskite and bottom silicon heterojunction solar cells varying with time. (d) Simulated efficiency (left) of perovskite/silicon monolithic 2T TSCs with an efficiency of 23.6%¹⁰ varying with time, compared with that of 4T TSCs and their efficiency difference ΔEff (right). Relative efficiency losses of different latitudes based on the perovskite/silicon monolithic TSCs with an efficiency of (e) 23.6%¹⁰ and (f) 25.2%,¹¹ using 4T TSCs at vertical incidence as reference.

time and plotted the solar irradiance varying with time, as shown in Figure 1b, on March 20, June 20, Sept 20, and Dec 20, respectively. These days are the representative days of the spring, summer, autumn, and winter seasons of the Northern Hemisphere. When the intensity of solar irradiance is lower than 50 W/m^2 (the dashed line), we think that the sun sets and module is not working.

Thereafter, we extracted the EQE spectra from two kinds of current world record perovskite/silicon monolithic TSCs with efficiencies of 23.6%¹⁰ and 25.2%¹¹ for different textured front surfaces (we have noticed that Oxford PV has announced an efficiency of 28%, but there are no EQE data reported¹⁷). Based on the solar spectra and the EQE spectra ($\text{EQE}(\lambda)$), J_{SC} varying with time can be calculated using eq 1

$$J_{SC}(t) = \frac{q}{hc} \int \lambda E(\lambda, t) \text{EQE}(\lambda) d\lambda \quad (1)$$

where $E(\lambda, t)$ is the incident photon energy flux of different time t and q is the electron charge.

Next, the open-circuit voltage (V_{OC}) calculated from the J_{SC} by the Shockley diode equation is given as

$$V_{OC}(t) = \frac{k_B T}{q} \ln \left(\frac{J_{SC}(t)}{J_0} + 1 \right) \quad (2)$$

where k_B is the Boltzmann constant and T is the room temperature (298 K). J_0 is the diode saturation current density which can be obtained from experimental results: for different top perovskite cells, $J_0^{(\text{perovskite})}$ was derived from the current density–voltage (J – V) curve of the perovskite solar cells acquired from recent literature;³¹ while $J_0^{(\text{Si})}$ was derived from the world record silicon heterojunction solar cell reported by Masuko et al.^{32,33} with $V_{OC} = 0.74$ V and $J_{SC} = 41.8$ mA/cm². The V_{OC} of perovskite/silicon monolithic TSCs is calculated by adding the V_{OC} 's of two individual subcells, while the J_{SC} of TSCs is the smaller value of two subcells. Because of the incident power varying with time and geographic position, we employed the incident power under standard test conditions as a reference standard in order to make the efficiency comparable. Given that the FF is constant with time t , the efficiency η of the simulated solar cell based on incident power under standard test conditions can be obtained by

$$\eta(t) = \frac{FF \times J_{SC}(t) \times V_{OC}(t)}{0.1 \text{ W/cm}^2} \quad (3)$$

We calculated in Figure 1c, the J_{SC} of both subcells based on perovskite/silicon monolithic TSCs with an efficiency of 23.6% varying with time on June 20. Obviously, the best matched times are at 8 and 16 o'clock. When time is between 8 and 16 o'clock, the J_{SC} 's of bottom silicon subcell are lower than those of top perovskite subcell. So, the current mismatch is existing at most time in a day. Figure 1d shows the efficiency of the perovskite/silicon monolithic 2T TSCs varying with time based on the yielded J_{SC} in Figure 1c, together with the results of mechanically stacked 4T TSCs for comparison. We can see that the efficiencies of 2T TSCs are obviously lower than those of 4T TSCs, with the average absolute efficiency difference ΔEff about 1.6% (relative efficiency \approx 7%). The efficiencies of 2T TSCs are close to those of 4T TSCs only at 8 and 16 o'clock when the J_{SC} 's of both subcells are almost equal. We could finally show in Figure 1e,f the relative efficiency losses in the two typical perovskite/silicon monolithic TSCs with efficiencies of 23.6¹⁰ and 25.2%¹¹ at different latitudes of 0°N, 30°N, and 60°N and different dates of March 20, June 20, Sept 20, and Dec 20. It is clear that the relative efficiency losses gradually become larger as the latitude goes up, and the relative efficiency losses are always greater than 5% (can be even \sim 15% in winter) which are too large for practical application.

3. SIMULATION METHODS AND VALIDATION

In order to optimize efficiency losses, we need to have the EQE spectra of perovskite/silicon monolithic TSCs varying with incident angle θ . However, the EQE measurement for individual subcells is not suitable for perovskite/silicon monolithic TSCs. The EQE spectra of tandem cells are normally measured by using strong blue and red light biases to saturate the complementary subcells,^{10,11} with additional weak light to achieve the EQE spectra of corresponding subcells. In our previous paper,²⁶ we have elaborated that the simulated absorbance spectra of TSCs calculated by the finite-difference time-domain (FDTD) method can correctly show the tendency of EQE spectra at vertical incidence. On this account, it may be suitable and accurate to accomplish the task by using the simulated absorbance spectra varying with incident angle θ in substitute of the EQE spectra.

For the sake of verifying simulation validation of the absorbance spectra varying with incident angle θ , we have first fabricated both two single junction solar cells of a silicon heterojunction and perovskite solar cells, respectively. For silicon heterojunction solar cells, as shown in Figure 2a, the

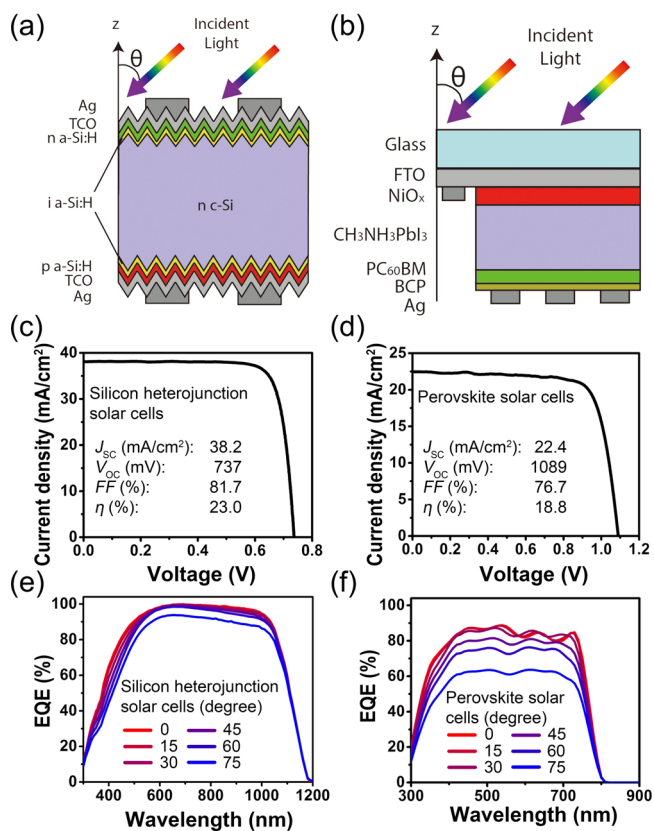


Figure 2. Schematic diagrams of the (a) silicon heterojunction solar cell and (b) perovskite solar cell. The parameter θ denotes incident angle in the study. J – V characteristics of the (c) silicon heterojunction solar cell and (d) perovskite solar cell. Measured EQE spectra of the (e) silicon heterojunction solar cell and (f) perovskite solar cell varying with incident angle θ .

used substrates were n-type c-Si wafers. Both n a-Si:H (\sim 10 nm)/i a-Si:H (\sim 5 nm) and p a-Si:H (\sim 10 nm)/i a-Si:H (\sim 5 nm) stack layers were deposited on the front and rear sides of the cells at a substrate temperature of 200 °C via plasma-enhanced chemical vapor deposition. Tungsten-doped tin oxide ($\text{In}_2\text{O}_3\text{:W}$) was deposited on both sides of the substrates as transparent conductive oxide (TCO) layers and antireflection layers by a reactive plasma deposition system. Finally, silver electrodes were screen printed on both sides. The details can be found in our previous paper.²⁷ The efficiency of our silicon solar cells (size 156 mm \times 156 mm) is about 23.0% measured under the AM 1.5 G spectrum. For perovskite solar cells, as shown in Figure 2b, the used substrates were the cleaned patterned fluorine-doped tin oxide ($\text{In}_2\text{O}_3\text{:F}$, a kind of TCO)/glass substrates. A NiO_x film was deposited on the substrates by our electrochemical deposition method.³⁴ Then, a perovskite layer was prepared by a one-step method³⁵ upon the NiO_x layer. Thereafter, PC_{60}BM and BCP layers (\sim 10 nm) were deposited successively on the perovskite layer by spin-coating. Finally, the silver electrode was deposited using thermal evaporation. Please refer to ref 34 for details. The efficiency of our prepared perovskite solar cells (size 5 mm \times 5

mm) is about 18.8% measured under a standard 1 sun AM 1.5 G solar simulator. The corresponding current J – V characteristics of both single junction solar cells are shown in Figure 2c,d.

We have further measured the EQE spectra of both the silicon heterojunction and perovskite solar cells by varying incident angle θ . We have given the definition of incident angle θ in Figure 2a,b, which is equal to the intersection angle between the incident light direction and the positive z direction. For silicon heterojunction solar cells, from Figure 2e, it is shown that the EQE spectra changes slightly at light incident angle θ ranging from 0 to 60°, with the main difference at the wavelength ranging from 400 to 600 nm. However, the EQE spectra decrease quickly when θ increases to 75°. The yielded J_{SC} 's of different incident angle θ 's, in Figure 2e, range from 40.34 to 36.64 mA/cm². For perovskite solar cells, Figure 2f shows that when the incident angle θ is smaller than 45°, the EQE spectra drop very slightly with increasing θ . Moreover, it decreases dramatically at light incident angle θ ranging from 45 to 75°. The resulted J_{SC} 's of different incident angle θ 's in Figure 2f range from 20.64 to 14.95 mA/cm². Because of different textured structures and refractive indexes, there are obvious differences about EQE spectra of the silicon heterojunction and perovskite solar cells with varying θ .

Based on those EQE data and structures of individual subcells, as shown in Figure 2, we employed the FDTD simulation package in Lumerical FDTD Solutions software (version 8.17.1072, 2017a) to perform optical calculations. The incident light plane wave was set to have an amplitude of one (with λ between 300 and 1200 nm) and was oriented toward the negative z -direction (see Figure 2a,b). The incident angle θ was changed by tuning the number of “angle theta” in option “Source”. In addition, the polarization angle in FDTD was set to be 45° as the consequence of averaging P polarization and S polarization.²⁷ We swept the wavelength every 10 nm from 300 to 1200 nm. We obtained the normalized reflectance $R(\lambda)$ using a frequency-domain transmission monitor set on the top surface of the solar cell. We used the “Power absorbed” (P_{abs}) analysis group in the FDTD package to get the absorptance of specific layers including the silicon and perovskite layers.²⁶ Perfectly matched layer boundary conditions were used in the z -direction and Bloch boundary conditions were used in the x – y directions. In order to simplify the simulations, we assumed the internal quantum efficiency of unity in the simulated materials.

The simulated silicon heterojunction solar cell, of which a schematic drawing is shown in Figure 2a, consists of a 150 nm thick TCO layer with a carrier concentration of 5.0×10^{19} cm⁻³, a 180 μ m thick n-type c-Si with micron-sized pyramid-textured surfaces, (ca. 5.0 μ m) and a 100 nm thick TCO with a carrier concentration of 2.0×10^{20} cm⁻³. Other amorphous silicon thin film layers whose thicknesses were less than 10 nm were eliminated from our optical model. The perovskite solar cell, of which a schematic drawing is shown in Figure 2b, consists of a 150 nm thick TCO with a carrier concentration of 2.0×10^{20} cm⁻³, a 10 nm thick electron transport layer of PC₆₀BM, a 460 nm thick perovskite layer (MAPbI₃, with a band gap of 1.56 eV), a 50 nm thick hole transport layer of NiO_x and an 80 nm thick silver electrode. The refractive indexes and extinction coefficients of all materials were obtained from the recent literatures.^{36–40}

The simulated absorptances of silicon and perovskite solar cells are shown in Figure 3a,b, respectively. We have already

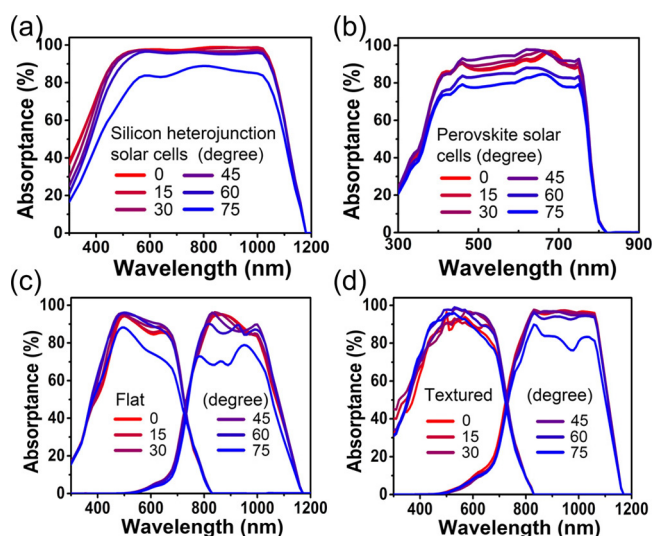


Figure 3. Simulated absorptance of the (a) silicon heterojunction solar cell and (b) perovskite solar cell varying with incident angle θ . Simulated absorptance of perovskite/silicon monolithic TSCs varying with incident angle θ (c) with a flat front surface and a textured rear surface (ca. 5.0 μ m) and (d) with textured front (ca. 1.0 μ m) and rear (ca. 5.0 μ m) surfaces.

assumed that every absorbed photon generates a hole–electron pair, so the simulated absorptances are equal to the EQE spectra. It is clear that the simulated absorptances of both solar cells are similar to their EQE spectra (see Figure 2e,f) in tendency with incident angle θ . For silicon solar cells, the simulated J_{SC} 's at incident angle θ ranging from 0 to 75° range from 41.06 to 34.58 mA/cm². They are very close to the J_{SC} calculated based on EQE spectra. For perovskite solar cells, the J_{SC} 's at incident angle θ ranging from 0 to 75° range from 23.15 to 19.74 mA/cm². They are larger than the J_{SC} calculated from EQE spectra. The main reason for the difference is that the quality of our prepared perovskite solar cells is obviously unable to reach that of an ideal sample. Although there is some difference between the absorptance and EQE spectra, they can also correctly show the tendency varying with incident angle θ . So, this simulated method can still be used to achieve optical characteristics of perovskite/silicon monolithic TSCs varying with incident angle θ .

Finally, we could calculate the absorptance spectra varying with incident angle θ from the reported perovskite/silicon monolithic TSCs^{10,11} by optimizing some parameters such as carrier concentrations and thicknesses of each layer. The simulated perovskite/silicon monolithic TSC consists of an antireflective layer (150 nm, LiF)/a TCO layer (150 nm, with a carrier concentration of 5×10^{19} cm⁻³)/an electron transport layer (10 nm, PC₆₀BM)/a perovskite layer (460 nm, Cs_{0.17}FA_{0.83}Pb(Br_{0.17}I_{0.83})₃, with a band gap of 1.63 eV)/a hole transport layer (28 nm, NiO)/a TCO layer (20 nm, with a carrier concentration of 5.0×10^{20} cm⁻³)/a c-Si layer (280 μ m)/an electrode layer (200 nm, Ag). The schematic can be seen in our previous work as ref 26. Figure 3c,d shows the calculated absorptance of TSCs varying with incident angle θ . For Figure 3c, the TSC includes a polished front surface and a micron-sized pyramid-textured rear surface (ca. 5.0 μ m), while for Figure 3d, the TSC features micron-sized pyramid-textured

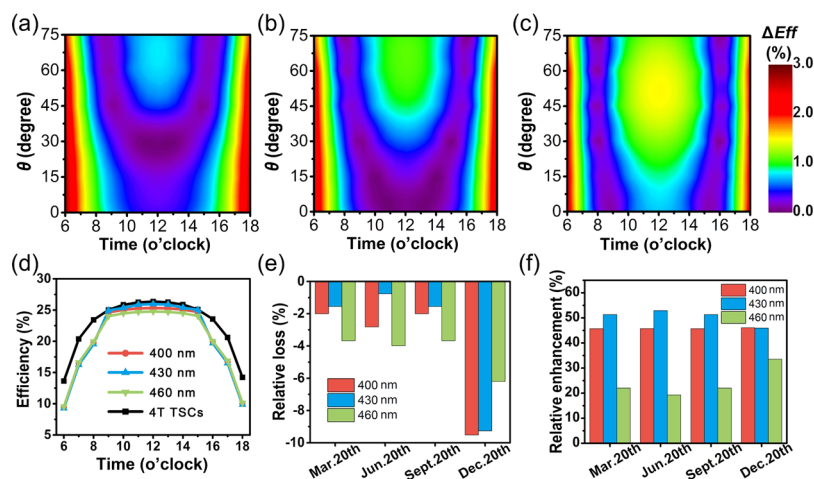


Figure 4. Contour of the efficiency difference ΔEff in perovskite/silicon heterojunction monolithic TSCs with a flat front surface and a micron-sized pyramid-textured rear surface (ca. $5.0\ \mu\text{m}$) at different times and incident angle θ 's on June 20 at three different perovskite layer thicknesses of (a) 400, (b) 430, and (c) 460 nm, respectively. (d) Optimized efficiency of perovskite/silicon heterojunction monolithic TSCs with a flat front surface and a micron-sized pyramid-textured rear surface (ca. $5.0\ \mu\text{m}$) at different times on June 20. (e) Relative efficiency loss and (f) relative-matched current enhancement of perovskite/silicon heterojunction monolithic TSCs with a flat front surface and a micron-sized pyramid-textured rear surface (ca. $5.0\ \mu\text{m}$) on March 20, June 20, Sept 20, and Dec 20, using 4T TSCs at vertical incidence and mismatched current value at vertical incidence as references, respectively.

front (ca. $1.0\ \mu\text{m}$) and rear (ca. $5.0\ \mu\text{m}$) surfaces. It is clear that the simulated absorptances of both subcells decrease very significantly with the incident angle θ larger than 60° , and the variation is more drastic in the polished front surface case (Figure 3c) than that in the micron-sized pyramid-textured front surface case shown in Figure 3d. However, when the incident angle θ is smaller than 60° , the absorptance of silicon subcells keeps almost unchanged, while the absorptance of perovskite subcells raises slightly with increasing θ at wavelength ranging from 500 to 700 nm as a result of a longer path in the perovskite layer.

4. OPTIMIZATION AT OBLIQUE INCIDENCE

In previous sections, we have calculated the efficiency losses at vertical incidence and yielded the simulated absorptance spectra of perovskite/silicon heterojunction monolithic TSCs varying with incident angle θ . Now, we calculate the efficiency losses of perovskite/silicon monolithic TSCs at oblique incidence. By using the methods reported in Section 2, we first examined different absorptance spectra of perovskite/silicon heterojunction monolithic TSCs with a flat front surface and a micron-sized pyramid-textured rear surface (ca. $5.0\ \mu\text{m}$) by tuning the thicknesses of the perovskite layer. Then, we employed eq 1 to calculate the J_{SC} varying with time and incident angle θ by replacing EQE spectra (EQE(λ)) with absorptance spectra $P_{\text{abs}}(\lambda, t)$. Thereafter, by using eqs 2 and 3, we could calculate the V_{OC} and efficiency η to form corresponding data matrixes varying with time t and incident angle θ , together with the results of 4T TSCs for comparison. Finally, we achieved the efficiency difference, relative efficiency losses, and relative-matched current enhancement based on the yielded data matrixes.

Figures 4a–c shows the contour of efficiency difference ΔEff in perovskite/silicon monolithic TSCs with a flat front surface on June 20 at three different thicknesses of perovskite layers of 400, 430, and 460 nm, respectively. The corresponding calculated J_{SC} 's of their perovskite/silicon subcells under the AM 1.5 G spectrum at vertical incidence are 18.2/19.1, 18.5/

18.8, and 18.8/18.4 mA/cm^2 , respectively. Obviously, the J_{SC} of perovskite subcells gradually increases with the thickness of perovskite layer. In Figure 4a, the purple area that the efficiency losses are ca. zero is mainly at incident angle θ ranging from 30 to 75° . However, the purple area expands at incident angle θ ranging from 0 to 75° in Figure 4b. The reduced efficiency loss of perovskite/silicon monolithic TSCs in Figure 4b is due to the fact that the appropriate mismatch of J_{SC} under the AM 1.5 G spectrum makes the J_{SC} easier to match at small incident angle θ under real solar spectra. However, in Figure 4c, because the J_{SC} of perovskite subcells is larger than that of silicon subcells at vertical incidence, the mismatch of J_{SC} 's will become more serious when the incident angle θ increases. As a result, it is impossible to minimize the efficiency losses to zero at time ranging from 10 to 14 o'clock, and the best case is the perovskite/silicon monolithic TSCs with perovskite layer thickness of 430 nm.

We have further shown in Figure 4d, the simulated efficiency extracted from efficiency matrixes based on the optimized incident angle θ 's on June 20. It is found that the efficiencies of perovskite/silicon 2T TSCs with a perovskite layer thickness of 430 nm are close to those of 4T TSCs at a time ranging from 9 to 15 o'clock. The highest efficiency of perovskite/silicon monolithic TSCs is 26.4% at 12 o'clock on June 20. Figure 4e,f shows the relative efficiency losses and relative-matched current enhancements on March 20, June 20, Sept 20, and Dec 20. The relative-matched current enhancement is calculated by dividing the mismatched value of J_{SC} 's at optimized incident angle θ 's by those at vertical incidence. Compared with the efficiency losses at vertical incidence as shown in Figure 1e,f, all perovskite/silicon monolithic TSCs with three different perovskite layer thicknesses at oblique incidence have lower relative efficiency losses over the course of a year. The relative efficiency losses are less than 2% (can be $<10\%$ in winter) at a perovskite layer thickness of 430 nm. The decrease of the relative efficiency losses is due to the fact that the matched current is significantly enhanced at oblique incidence as shown in Figure 4f. The relative-matched current

enhancement is always greater than 40% at a perovskite layer thickness of 430 nm.

In Figure 4, we have succeeded in reducing the efficiency losses of perovskite/silicon heterojunction monolithic TSCs with a flat front surface by tuning the incident angle θ and the thickness of the perovskite layer. However, the efficiency (maximum $\sim 26.4\%$ at 12 o'clock) is still not high enough because of current losses caused by surface reflection and parasitic absorbance. Therefore, we have identified, as shown in Figure 5a, the current losses J_{LOSS} in different layers varying

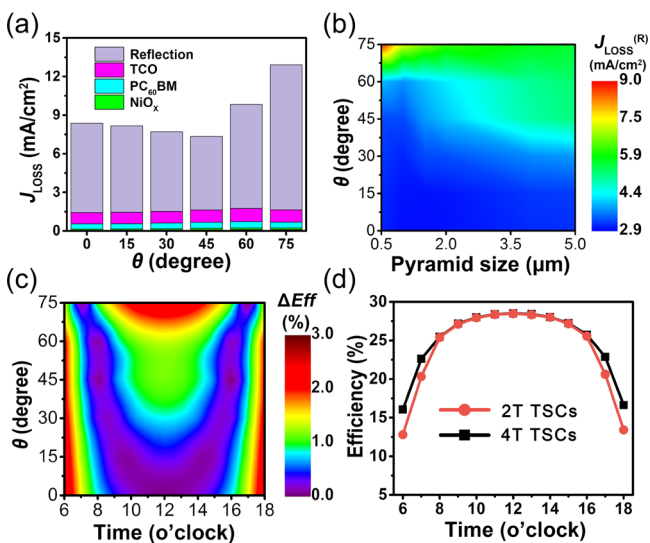


Figure 5. (a) Current losses J_{LOSS} caused by different layers in perovskite/silicon heterojunction monolithic TSCs with a flat front surface and a micron-sized pyramid-textured rear surface (ca. $5.0 \mu\text{m}$) at a perovskite layer thickness of 430 nm varying with incident angle θ . (b) Contour of current losses caused by reflection ($J_{\text{LOSS}}^{\text{R}}$) in perovskite/silicon heterojunction monolithic TSCs with a micron-sized pyramid-textured rear surface (ca. $5.0 \mu\text{m}$) at different pyramid period sizes of the textured front surface and incident angle θ 's. (c) Contour of the efficiency difference ΔEff in perovskite/silicon heterojunction monolithic TSCs with a pyramid textured front surface ($\sim 1.0 \mu\text{m}$), a micron-sized pyramid-textured rear surface (ca. $5.0 \mu\text{m}$) and the best perovskite layer thickness ($\sim 620 \text{ nm}$) on June 20. (d) Simulated efficiency extracted from efficiency matrixes based on the optimized incident angle θ 's of perovskite/silicon heterojunction monolithic 2T TSCs with a quasi-omnidirectional pyramid-textured front surface ($\sim 1.0 \mu\text{m}$) and a micron-sized pyramid-textured rear surface (ca. $5.0 \mu\text{m}$) on June 20, together with the case of 4T TSCs for comparison.

with incident angle θ . Clearly, the cell surface reflection plays the most important roles in the current losses. Also, the surface reflection loss is found to decrease gradually at incident angle θ ranging from 0 to 45° , and then it increases visibly at incident angle θ ranging from 45° to 75° , which can well explain the mismatched efficiency at time ranging from 6 to 9 and 15 to 18 o'clock in Figure 4d. From Figure 5a, we can conclude that optimizing surface reflection especially at high incident angle θ is the best way to improve the efficiency losses of the perovskite/silicon heterojunction monolithic TSCs at oblique incidence.

Many research groups including ours^{10,11,25,26,41,42} reported that texturing the front surface was the best way to minimize the reflection by experiment and simulation. Nevertheless, there is no reflection result on pyramid sizes of the textured

front surface at different incident angle θ 's. In Figure 5b, we illustrated the calculated current loss caused by reflection ($J_{\text{LOSS}}^{\text{R}}$) with different front pyramid period sizes and incident angle θ 's. We assumed that the characteristic base angle of the pyramid-texture was close to $50\text{--}52^\circ$, as was used in the literature.⁴³ It is found that different pyramid-textured sizes can all reduce $J_{\text{LOSS}}^{\text{R}}$ to ca. 2.9 mA/cm^2 at incident angle θ ranging from 0 to 30° , clearly demonstrate that texturing the front surface is effective in reducing the reflection. We also notice that smaller pyramid-textured sizes favor the reduced $J_{\text{LOSS}}^{\text{R}}$ at incident angle θ ranging from 30° to 75° , but $J_{\text{LOSS}}^{\text{R}}$ caused by the reflection increases significantly to ca. 9.0 mA/cm^2 at incident angle θ around 75° under the pyramid-textured size below $1.0 \mu\text{m}$. Such low reflectance over broad incident angle θ 's indicates that the perovskite/silicon monolithic TSCs with a pyramid-textured front surface ($\sim 1.0 \mu\text{m}$) have quasi-omnidirectional property.²⁷ Therefore, the best pyramid size of the textured front surface for application is ca. $1.0 \mu\text{m}$, where the optimized perovskite layer thickness is calculated to be 620 nm.

Figure 5c shows the contour of the efficiency difference ΔEff in perovskite/silicon heterojunction monolithic TSCs with a quasi-omnidirectional pyramid-textured front surface ($\sim 1.0 \mu\text{m}$) and the best perovskite layer thickness ($\sim 620 \text{ nm}$) on June 20. Compared with that in Figure 4b, the purple area that the efficiency losses are ca. zero expands toward a smaller incident angle and wider time range. Further evidence of the improvement can be found in Figure 5d, where the efficiency of perovskite/silicon heterojunction monolithic 2T TSCs is almost the same as that of 4T TSCs at time ranging from 8 to 16 o'clock. Therefore, the output of perovskite/silicon monolithic TSCs during the mid-part of the day on June 20 is as large as possible; meanwhile the efficiency losses during early and late day are also reduced. The best efficiency of monolithic TSCs is 28.6% at 12 o'clock on June 20 with the relative efficiency loss of near 0% compared with that ca. 0.8% in Figure 4e.

5. ENERGY OUTPUT ANALYSIS AND OPTIMIZED ΔJ_{SC}

From the above discussion, we have found a little current mismatch of two subcells in perovskite/silicon monolithic TSCs is better for achieving lower efficiency loss under solar spectra of latitude 30°N . In order to further analyze the total impact of a year, the relative efficiency loss at the location of latitude 30°N is shown in Figure 6a varying the J_{SC} difference (ΔJ_{SC}) of two subcells, using 4T TSCs at vertical incidence as references. The ΔJ_{SC} is defined by subtracting the J_{SC} 's of perovskite subcells from those of silicon subcells, which can be calculated by eq 1 varying the perovskite layer thickness in perovskite/silicon monolithic TSCs at vertical incidence under the AM 1.5 G spectrum. It is obvious that the relative efficiency losses of different seasons show different increasing and decreasing relationships varying with the ΔJ_{SC} . We have also calculated the annual energy output W in Figure 6a by eq 4

$$W = \int P_{\text{illum}} \times \eta(t) dt \quad (4)$$

where P_{illum} is defined to be 0.1 W/cm^2 according to standard testing conditions under the AM 1.5 G spectrum and $\eta(t)$ is the conversion efficiency of different time t calculated by eq 3. It is found that at the location of latitude 30°N , the annual energy output reaches its maximum of 962 kW h/m^2 at a ΔJ_{SC}

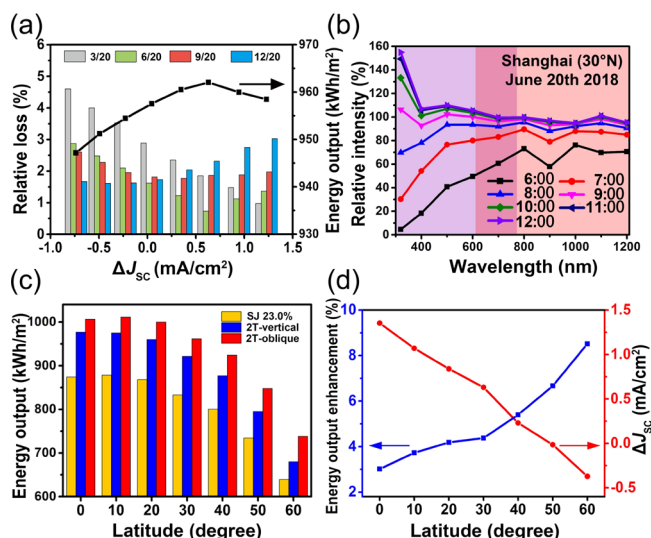


Figure 6. (a) Relative efficiency loss (left) vs ΔJ_{SC} of two subcells on March 20, June 20, Sept 20, and Dec 20 at the location of latitude 30°N , using 4T TSCs at vertical incidence as reference. Positive and negative ΔJ_{SC} 's represent that the J_{SC} 's of silicon subcells are higher and lower than those of perovskite subcells, respectively. Also shown is the corresponding annual energy output (right) varying with the ΔJ_{SC} of two subcells. (b) Relative intensity spectra obtained by dividing solar spectral irradiance on June 20 at the location of latitude 30°N by the AM 1.5 G spectrum. The light purple and light red areas represent the parts absorbed by perovskite and silicon subcells, respectively. (c) Annual energy outputs of three different solar cells varying with latitude at the North Hemisphere under clear-sky conditions: silicon single junction cells with efficiency of 23.0% (SJ 23.0%), perovskite/silicon monolithic TSCs at vertical incidence (2T-vertical), and at optimized oblique incidence (2T-oblique). (d) Energy output enhancement (left) and corresponding optimized ΔJ_{SC} (right) of the perovskite/silicon monolithic TSCs at optimized oblique incidence varying with latitude. Positive and negative ΔJ_{SC} 's represent that the J_{SC} 's of silicon subcells are higher and lower than that of perovskite subcells, respectively.

of ca. 0.63 mA/cm^2 , which is the best balance point of efficiency losses of a year.

The underlying cause of an optimized ΔJ_{SC} can be understood by the relative intensity spectra shown in Figure 6b obtained by dividing solar spectral irradiance at the location of latitude 30°N by the AM 1.5 G spectrum, taking June 20 as an example. Obviously, the part absorbed by perovskite subcells (light purple area) at a wavelength ranging from 300 to 780 nm changes more dramatically than that of silicon subcells (light red area) at a wavelength ranging from 600 to 1200 nm, which makes the optimization of ΔJ_{SC} extremely essential. The relative intensity at the light purple area absorbed by perovskite subcells at 12 o'clock (the energy output maximum point) is higher than 100%, which means that the solar spectra at 12 o'clock are brighter than those of the AM 1.5 G standard spectrum. However, for the light red area absorbed by silicon subcells, the solar spectra at 12 o'clock is close to those of the AM 1.5 G standard spectrum. Based on the previous analysis in Figures 4b and 5c, the optimized incident angle θ at 12 o'clock should be close to 0° (vertical incidence) in order to achieve the minimum efficiency losses. If the perovskite/silicon monolithic TSCs have the best matched J_{SC} 's of two subcells under the AM 1.5 G spectrum at vertical incidence, the corresponding J_{SC} 's of perovskite subcells will be higher than those of silicon subcells under solar spectra of

latitude 30°N at 12 o'clock. Therefore, in order to make the J_{SC} 's of two subcells match under solar spectra of latitude 30°N , the J_{SC} 's of the perovskite subcells under the AM 1.5 G spectrum should be lower than those of silicon subcells under the AM 1.5 G spectrum at vertical incidence, as observed a positive optimized ΔJ_{SC} of ca. 0.63 mA/cm^2 in Figure 6a.

Finally, we have expanded the study to the latitudes ranging from 0°N to 60°N . We show in Figure 6c, the annual energy output of three different devices (silicon single junction with efficiency of 23.0%, 2T TSCs at vertical incidence, 2T TSCs at optimized oblique incidence). Obviously, the annual energy output decreases as the latitude goes up, and the annual energy outputs of perovskite/silicon monolithic TSCs are higher than those of silicon single junction solar cells at any latitudes because of higher efficiency of perovskite/silicon monolithic TSCs. For perovskite/silicon monolithic TSCs, the annual energy output at optimized oblique incidence is higher than that at the vertical incidence case. The energy output enhancement and corresponding application values of optimized ΔJ_{SC} are shown in Figure 6d. Clearly, the optimized ΔJ_{SC} becomes smaller as the latitude goes up (the value can even be negative at a latitude of 60°N) due to the fact that solar spectra at short wavelengths decrease quickly as the latitude goes up. In contrast, the energy output enhancement gradually becomes larger as the latitude goes up. At latitude ranging from 0°N to 20°N (between the equator and the Tropic of Cancer), the energy output enhancement is relatively small ca. 3% because of fairly stable spectra of different seasons. However, the energy output enhancement can be even $\sim 9\%$ at latitude of 60°N , which will restrict significantly the application of perovskite/silicon monolithic TSCs if not optimizing. The optimized ΔJ_{SC} illustrated in Figure 6d provides a guideline for the design of perovskite/silicon monolithic TSCs with the best annual energy output at different latitudes in the world.

6. CONCLUSIONS

In summary, we have successfully analyzed the efficiency losses of perovskite/silicon monolithic TSCs at vertical and oblique incidence under real solar spectra at different times in a year under clear-sky conditions. We have found that the average absolute efficiency difference of best-matched perovskite/silicon monolithic TSCs with a flat front surface on June 20 is about 1.6% (relative efficiency $\approx 7\%$) under real spectra at vertical incidence, which is too large for practical application. However, by employing the optimized incident angle θ , the quasi-omnidirectional textured front surface ($\sim 1.0 \mu\text{m}$) and the thickness of the perovskite layer ($\sim 620 \text{ nm}$), the relative efficiency loss can be reduced to near 0% at oblique incidence on June 20. Furthermore, we have calculated the annual energy output maximum of 962 kW h/m^2 at the optimized ΔJ_{SC} of ca. 0.63 mA/cm^2 at the location of latitude of 30°N . Finally, we have shown the energy output enhancement and corresponding values of optimized ΔJ_{SC} by expanding the study to latitudes from 0°N to 60°N . These results could hopefully improve the performance of perovskite/silicon monolithic TSCs in practical application at different locations and accelerate the industrialization path of perovskite/silicon monolithic TSCs.

AUTHOR INFORMATION

Corresponding Author

*E-mail: wzshen@sjtu.edu.cn.

ORCID 

Lixiang Ba: 0000-0003-1118-0054

Tun Wang: 0000-0002-0020-3268

Notes

The authors declare no competing financial interest.

ACKNOWLEDGMENTS

This work was supported by the Natural Science Foundation of China (11834011 and 11674225) and the Major State Basic Research Development Program of China (no. 2018YFB1500501).

REFERENCES

- (1) Werner, J.; Niesen, B.; Ballif, C. Perovskite/Silicon Tandem Solar Cells: Marriage of Convenience or True Love Story?—An Overview. *Adv. Mater. Interfaces* **2018**, *5*, 1700731.
- (2) Lee, J.-W.; Hsieh, Y.-T.; De Marco, N.; Bae, S.-H.; Han, Q.; Yang, Y. Halide Perovskites for Tandem Solar Cells. *J. Phys. Chem. Lett.* **2017**, *8*, 1999–2011.
- (3) Todorov, T. K.; Bishop, D. M.; Lee, Y. S. Materials perspectives for next-generation low-cost tandem solar cells. *Sol. Energy Mater. Sol. Cells* **2018**, *180*, 350–357.
- (4) Schnabel, M.; Rienacker, M.; Warren, E. L.; Geisz, J. F.; Peibst, R.; Stradins, P.; Tamboli, A. C. Equivalent Performance in Three-Terminal and Four-Terminal Tandem Solar Cells. *IEEE J. Photovolt.* **2018**, *8*, 1584–1589.
- (5) Santbergen, R.; Uzu, H.; Yamamoto, K.; Zeman, M. Optimization of Three-Terminal Perovskite/Silicon Tandem Solar Cells. *IEEE J. Photovolt.* **2019**, *9*, 446–451.
- (6) Warren, E. L.; Deceglie, M. G.; Rienacker, M.; Peibst, R.; Tamboli, A. C.; Stradins, P. Maximizing Tandem Solar Cell Power Extraction Using a Three-Terminal Design. *Sustainable Energy Fuels* **2018**, *2*, 1141–1147.
- (7) Mailoa, J. P.; Bailie, C. D.; Johlin, E. C.; Hoke, E. T.; Akey, A. J.; Nguyen, W. H.; McGehee, M. D.; Buonassisi, T. A 2-Terminal Perovskite/Silicon Multijunction Solar Cell Enabled by a Silicon Tunnel Junction. *Appl. Phys. Lett.* **2015**, *106*, 121105.
- (8) Werner, J.; Weng, C.-H.; Walter, A.; Fesquet, L.; Seif, J. P.; De Wolf, S.; Niesen, B.; Ballif, C. Efficient Monolithic Perovskite/Silicon Tandem Solar Cell with Cell Area > 1 cm². *J. Phys. Chem. Lett.* **2016**, *7*, 161–166.
- (9) Wu, Y.; Yan, D.; Peng, J.; Duong, T.; Wan, Y.; Phang, S. P.; Shen, H.; Wu, N.; Barugkin, C.; Fu, X.; et al. Monolithic Perovskite/Silicon-Homojunction Tandem Solar Cell with Over 22% Efficiency. *Energy Environ. Sci.* **2017**, *10*, 2472–2479.
- (10) Bush, K. A.; Palmstrom, A. F.; Yu, Z. J.; Boccard, M.; Cheacharoen, R.; Mailoa, J. P.; McMeekin, D. P.; Hoye, R. L. Z.; Bailie, C. D.; Leijtens, T.; et al. 23.6%-Efficiency Monolithic Perovskite/Silicon Tandem Solar Cells with Improved Stability. *Nat. Energy* **2017**, *2*, 17009.
- (11) Sahli, F.; Werner, J.; Kamino, B.; Brauning, M.; Monnard, R.; Salomon, B.; Barraud, L.; Ding, L.; Leon, J.; Sacchetto, D.; et al. Fully Textured Monolithic Perovskite/Silicon Tandem Solar Cells with 25.2% Power Conversion Efficiency. *Nat. Mater.* **2018**, *17*, 820–826.
- (12) Bush, K. A.; Manzoor, S.; Frohna, K.; Yu, Z.; Raiford, J.; Palmstrom, A.; Wang, H.; Prasanna, R.; Bent, S. F.; Holman, Z. C.; et al. Minimizing Current and Voltage Losses to Reach 25% Efficient Monolithic Two-Terminal Perovskite-Silicon Tandem Solar Cells. *ACS Energy Lett.* **2018**, *3*, 2173–2180.
- (13) Köhnen, E.; Jošt, M.; Morales-Vilches, A. B.; Tockhorn, P.; Al-Ashouri, A.; Macco, B.; Kegelmann, L.; Korte, L.; Rech, B.; Schlattmann, R.; et al. Highly Efficient Monolithic Perovskite Silicon Tandem Solar Cells: Analyzing the Influence of Current Mismatch on Device Performance. *Sustainable Energy Fuels* **2019**, *3*, 1995–2005.
- (14) Bonnet-Eymard, M.; Boccard, M.; Bugnon, G.; Sculati-Meillaud, F.; Despeisse, M.; Ballif, C. Optimized Short-circuit Current Mismatch in Multi-junction Solar Cells. *Sol. Energy Mater. Sol. Cells* **2013**, *117*, 120–125.
- (15) Yu, Z.; Leilaieoun, M.; Holman, Z. Selecting Tandem Partners for Silicon Solar Cells. *Nat. Energy* **2016**, *1*, 16137.
- (16) Yoshikawa, K.; Kawasaki, H.; Yoshida, W.; Irie, T.; Konishi, K.; Nakano, K.; Uto, T.; Adachi, D.; Kanematsu, M.; Uzu, H.; et al. Silicon Heterojunction Solar Cell with Interdigitated Back Contacts for a Photoconversion Efficiency Over 26%. *Nat. Energy* **2017**, *2*, 17032.
- (17) Taiyangnews for 28% Efficiency for Oxford PV Perovskite Cell. <http://taiyangnews.info/technology/28-efficiency-for-oxford-pv-perovskite-cell/> (accessed 05, 2019).
- (18) Taiyangnews for 27.1% Perovskite/Si Tandem Cell from IMEC. <http://taiyangnews.info/technology/27-1-perovskites-tandem-cell-from-imec/> (accessed 05, 2019).
- (19) Sahli, F.; Kamino, B. A.; Werner, J.; Bräuninger, M.; Paviet-Salomon, B.; Barraud, L.; Monnard, R.; Seif, J. P.; Tomasi, A.; Jeangros, Q.; et al. Improved Optics in Monolithic Perovskite/Silicon Tandem Solar Cells with a Nanocrystalline Silicon Recombination Junction. *Adv. Energy Mater.* **2018**, *8*, 1701609.
- (20) Zheng, J.; Lau, C.; Mehrvarz, H.; Ma, F.; Jiang, Y.; Deng, X.; Soeriyadi, A.; Kim, J.; Zhang, M.; Hu, L.; et al. Large Area Efficient Interface Layer Free Monolithic Perovskite/Homo-Junction-Silicon Tandem Solar Cell with Over 20% Efficiency. *Energy Environ. Sci.* **2018**, *11*, 2432–2443.
- (21) Kamino, B. A.; Paviet-Salomon, B.; Moon, S.-J.; Badel, N.; Levrat, J.; Christmann, G.; Walter, A.; Faes, A.; Ding, L.; Diaz Leon, J. J.; et al. Low-Temperature Screen-Printed Metallization for the Scale-Up of Two-Terminal Perovskite-Silicon Tandems. *ACS Appl. Energy Mater.* **2019**, *2*, 3815–3821.
- (22) Dupré, O.; Niesen, B.; De Wolf, S.; Ballif, C. Field Performance versus Standard Test Condition Efficiency of Tandem Solar Cells and the Singular Case of Perovskites/Silicon Devices. *J. Phys. Chem. Lett.* **2018**, *9*, 446–458.
- (23) Jošt, M.; Köhnen, E.; Morales, A.; Lipovsek, B.; Jager, K.; Macco, B.; Ashouri, A.; Krc, J.; Korte, L.; Rech, B.; et al. Textured Interfaces in Monolithic Perovskite/Silicon Tandem Solar Cells: Advanced Light Management for Improved Efficiency and Energy Yield. *Energy Environ. Sci.* **2018**, *11*, 3511–3523.
- (24) Schmagar, R.; Langenhorst, M.; Lehr, J.; Lemmer, U.; Richards, B. S.; Paetzold, U. W. Methodology of energy yield modelling of perovskite-based multi-junction photovoltaics. *Opt. Express* **2019**, *27*, A507–A523.
- (25) Shi, D.; Zeng, Y.; Shen, W. Perovskite/c-Si tandem Solar Cell with Inverted Nanopyramids: Realizing High Efficiency by Controllable Light Trapping. *Sci. Rep.* **2015**, *5*, 16504.
- (26) Ba, L.; Liu, H.; Shen, W. Perovskite/c-Si Tandem Solar Cells with Realistic Inverted Architecture: Achieving High Efficiency by Optical Optimization. *Prog. Photovolt. Res. Appl.* **2018**, *26*, 924–933.
- (27) Zhong, S.; Wang, W.; Tan, M.; Zhuang, Y.; Shen, W. Realization of Quasi-Omnidirectional Solar Cells with Superior Electrical Performance by All-Solution-Processed Si Nanopyramids. *Adv. Sci.* **2017**, *4*, 1700200.
- (28) Zhuang, Y. F.; Zhong, S. H.; Liang, X. J.; Kang, H. J.; Li, Z. P.; Shen, W. Z. Application of SiO₂ passivation technique in mass production of silicon solar cells. *Sol. Energy Mater. Sol. Cells* **2019**, *193*, 379–386.
- (29) Reda, I.; Andreas, A. Solar Position Algorithm for Solar Radiation Applications. *Sol. Energy* **2004**, *76*, 577–589.
- (30) Al Garni, H. Z.; Awasthi, A.; Wright, D. Optimal Orientation Angles for Maximizing Energy Yield for Solar PV in Saudi Arabia. *Renewable Energy* **2019**, *133*, 538–550.
- (31) Werner, J.; Barraud, L.; Walter, A.; Bräuninger, M.; Sahli, F.; Sacchetto, D.; Tétreault, N.; Paviet-Salomon, B.; Moon, S.-J.; Allebé, C.; et al. Efficient Near-Infrared-Transparent Perovskite Solar Cells Enabling Direct Comparison of 4-Terminal and Monolithic Perovskite/Silicon Tandem Cells. *ACS Energy Lett.* **2016**, *1*, 474–480.
- (32) Masuko, K.; Shigematsu, M.; Hashiguchi, T.; Fujishima, F.; Kai, M.; Yoshimura, N.; Yamaguchi, T.; Ichihashi, Y.; Mishima, T.;

Matsubara, N.; et al. Achievement of More Than 25% Conversion Efficiency with Crystalline Silicon Heterojunction Solar Cell. *IEEE J. Photovolt.* **2014**, *4*, 1433–1435.

(33) Taguchi, M.; Yano, A.; Tohoda, S.; Matsuyama, K.; Nakamura, Y.; Nishiwaki, T.; Fujita, K.; Maruyama, E. 24.7% Record Efficiency HIT Solar Cell on Thin Silicon Wafer. *IEEE J. Photovolt.* **2014**, *4*, 96–99.

(34) Wang, T.; Ding, D.; Wang, X.; Zeng, R.; Liu, H.; Shen, W. High-Performance Inverted Perovskite Solar Cells with Mesoporous NiO_x Hole Transport Layer by Electrochemical Deposition. *ACS Omega* **2018**, *3*, 18434–18443.

(35) Yang, D.; Yang, R.; Ren, X.; Zhu, X.; Yang, Z.; Li, C.; Liu, S. F. Hysteresis-Suppressed High-Efficiency Flexible Perovskite Solar Cells Using Solid-State Ionic-Liquids for Effective Electron Transport. *Adv. Mater.* **2016**, *28*, 5206–5213.

(36) Palik, E. D.; Hunter, W. R. Lithium Fluoride (LiF). *Handbook of Optical Constants of Solids*; Academic Press: San Diego, 1985; pp 675–693.

(37) Holman, Z. C.; Filipič, M.; Descoedres, A.; De Wolf, S.; Smole, F.; Topič, M.; Ballif, C. Infrared Light Management in High-Efficiency Silicon Heterojunction and Rear-Passivated Solar Cells. *J. Appl. Phys.* **2013**, *113*, 013107.

(38) Campoy-Quiles, M.; Müller, C.; Garriga, M.; Wang, E.; Inganäs, O.; Alonso, M. I. On the complex refractive index of polymer:fullerene photovoltaic blends. *Thin Solid Films* **2014**, *571*, 371–376.

(39) Ndione, P. F.; Li, Z.; Zhu, K. Effects of alloying on the optical properties of organic–inorganic lead halide perovskite thin films. *J. Mater. Chem. C* **2016**, *4*, 7775–7782.

(40) Bakr, N. A.; Salman, S. A.; Shano, A. M. Effect of Co Doping on Structural and Optical Properties of NiO Thin Films Prepared by Chemical Spray Pyrolysis Method. *Int. Lett. Chem., Phys. Astron.* **2014**, *41*, 15–30.

(41) Santbergen, R.; Mishima, R.; Meguro, T.; Hino, M.; Uzu, H.; Blanker, J.; Yamamoto, K.; Zeman, M. Minimizing Optical Losses in Monolithic Perovskite/c-Si Tandem Solar Cells with a Flat Top Cell. *Opt. Express* **2016**, *24*, A1288–A1299.

(42) Mazzarella, L.; Werth, M.; Jäger, K.; Jošt, M.; Korte, L.; Albrecht, S.; Schlatmann, R.; Stannowski, B. Infrared Photocurrent Management in Monolithic Perovskite/Silicon Heterojunction Tandem Solar Cells by Using a Nanocrystalline Silicon Oxide Interlayer. *Opt. Express* **2018**, *26*, A487–A497.

(43) Baker-Finch, S. C.; McIntosh, K. R. Reflection Distributions of Textured Monocrystalline Silicon: Implications for Silicon Solar Cells. *Prog. Photovolt. Res. Appl.* **2013**, *21*, 960–971.